Steam whirl analysis in a high pressure cylinder of a turbo generator

Nicolò Bachschmid
Dept. of Mechanics
Politecnico di Milano
Milan, Italy
nicolo.bachschmid@polimi.it

Paolo Pennacchi
Dept. of Mechanics
Politecnico di Milano
Milan, Italy
paolo.pennacchi@polimi.it

Andrea Vania
Dept. of Mechanics
Politecnico di Milano
Milan, Italy
andrea.vania@polimi.it

Abstract

In this paper steam whirl instability occurrence and modelling is described. Some weak points in usual modelling and in standard stability criteria are discussed. The motivation of the present study is the case history of a steam turbine that experienced heavy steam whirl instability though the calculated stability margin was sufficiently high in design conditions. During the electrical load rise of a power plant, the 425MW steam turbo generator showed an unstable vibrational behaviour as soon as maximum output power was approached.
The combined effect of steam excitation (in bladed rows and in the steam glands) and of low damping in some of the oil film bearings was most likely the main cause of the observed malfunction. A model of the turbo generator has been set up, the steam whirl exciting force coefficients and the oil film bearing coefficients have been applied and eigenfrequencies and damping factors have been calculated. In order to check the accuracy of this calculation also another method based on energy balance has been used but very similar values have been obtained, confirming the accuracy of the standard stability evaluation approach. The calculation showed that the machine should have been stable, with a sufficient margin of stability, in design conditions. Therefore the steam whirl excitation models have been analysed for identifying possible weak points which could justify the discrepancies between experimental behaviour and calculated results.

Keywords: Steam whirl, instability, steam glands, rotor dynamics

1. Introduction

Turbo-machinery like steam turbines and gas compressors may experience unstable vibrations due to interaction between the whirling shaft and the surrounding fluid forces in correspondence of seals where the clearance between rotating and stationary parts are small. These unstable vibrations arise in steam turbines most likely close to the maximum power condition, when pressures and consequent flows are maxima. The vibration amplitudes reach very quickly high unacceptable values, the machines are shut down due to excessive vibration levels and can then be operated only at reduced power levels. The unstable vibrations occur at the shaft first bending natural frequency, and can be controlled only by the damping introduced by the oil film bearings, or by some additional external damping. When damping is insufficient, instability can be overcome only by modifying the seal geometry. Since the occurrence of this type of instability has limited the development of performances of turbo-machinery, many studies have been devoted in the last 45 years, depending on the development needs of high performance turbo-machinery. Several topics were considered: the analysis of steam whirl in steam turbines, the instabilities excited by air flow in the axial compressors of gas turbines, the instabilities excited by the fluid in labyrinth seals of high performance centrifugal gas compressors and the instability excited by the liquid in the seals of high performance centrifugal pumps. The need of tight clearances for the development of high efficiency steam turbines has increased the risk of occurrence of steam whirl, therefore higher accuracy in predicting instability is required.

Despite the fact that there is a consolidated knowledge about these problems, at least in the scientific community, there are still some weak points in modelling the steam whirl excitation, so that predictions of stability margins sometimes can fail.

The motivation of the present study is exactly a case history of a steam turbine that experienced a heavy steam whirl instability though the stability margin in design conditions, calculated by the turbine manufacturer according to a consolidated methodology, was sufficiently high. A twin turbine operated in the same conditions had no stability problems at all.

First the main results of the studies about instability excited by fluid flow over seals or blade rows in turbo-machinery are recalled. Then the recent steam whirl instability event on the turbine is described, the calculation results of standard modelling and stability margin evaluation are presented. Finally some possible weak points in standard modelling are identified, which could justify the discrepancies between calculation results and experimental evidence.

2. Steam whirl modelling

Unstable behaviour occurring in HP steam turbines was first analysed by Thomas [1] in Germany. He realized that the excitation was mainly due to the unequal leakage steam flow over blade rows. Krämer [2] used the model of Thomas for the blade row steam leakage forces, which excite forward whirl, and introduced the model of oil film bearings showing the combined effect on stability. He defined a linearized cross coupling stiffness coefficient K_{xy} (force in x direction due to shaft displacement in y direction) proportional to the equivalent tangential driving force acting on the stage

$$K_{xy} = k \frac{N}{\Omega D_m l} \tag{1}$$

where N is the power of the stage, D_m the mean diameter of the blade row, Ω the rotating speed, k a parameter which has to be calculated modelling the leakage flow over the blades (which depends obviously on the clearance) and l the length of the blade.

Reliable values of k are not given, but can be calculated with thermodynamic models of flow over blade rows. Eq. (1) can be explained as follows (see Figure 1): the offset blade row (assumed offset equal to δ) and the consequent clearance difference makes pressure p_1 greater than pressure p_2, therefore the tangential driving force F_1 is greater than F_2. The resultant force over the blade row F_y depends on offset δ in x direction and pushes the shaft in y direction, giving rise to the whirling motion. The cross coupled stiffness is obtained dividing F_y by δ.

Considering the complete blade row, expression (1) is derived, where k/l takes account of the unequal pressure distribution resulting from unequal clearance and leakage over the blade tips. Due to symmetry the same cross coupling coefficient K_{yx} is obviously obtained in vertical direction.

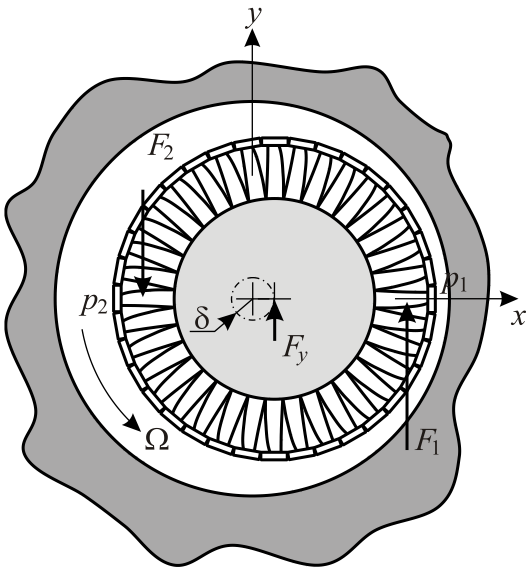

Figure 1: Forces applied to an offset blade row.

Values of k can be derived from diagrams in Thomas et al. [3]. These first experimental results, obtained with an offset rotating shaft, and not with a whirling shaft, showed that the forces are not linear with the shaft displacement, and are much higher for shrouded blades than for single standing blades, revealing the influence of the circumferential flow, which is also sometimes called the "gas bearing effect". This effect, which is present and well known in all hydraulic machinery, is obviously the only one present in the labyrinth seals where no blades are present (such as the balancing drum in HP steam turbines); it is mainly due to the rotation of the shaft and could be separated from leakage over blades effect which is apparently independent from rotation.

The gas bearing effect can be derived as follows: consider a shaft rotating at speed Ω inside the seal clearance (Figure 2). The centre of the shaft moves on a supposedly circular path of small radius δ with a whirling angular speed of ω.

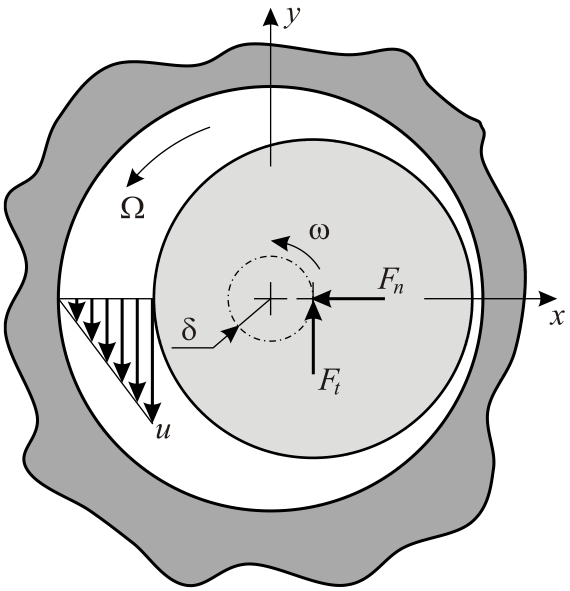

Figure 2: Forces on offset shaft in the seal clearance: the gas bearing effect.

In the position of Figure 2 the resultant fluid forces on the shaft are expressed by (see for instance [4]):

$$F_n = K_{xx}\,\delta + r_{xy}\,\omega\,\delta \tag{2}$$

$$F_t = K_{yx}\,\delta + r_{yy}\,\omega\,\delta \tag{3}$$

where damping and stiffness coefficients are calculated considering turbulent flow in a similar way to oil-film journal bearings.

The forces are rotating with speed ω: F_n contributes to the stiffness of the bearings while F_t, when directed as in Figure 2, is the destabilizing force which introduces energy in the whirling motion. If F_t is opposite, the energy is dissipated, but this does not occur in circular bearings. Stiffness and damping coefficients of (3) depend strongly on pre-swirl speed $\bar{u}$ which is the mean tangential flow inlet speed in the seal, where the flow should be almost axial, driven by the pressure drop. Pre-swirl is generated mainly by fluid layers trailed by friction from rotating surfaces, but depend on geometry and fluid conditions in the space before the seal, and can be reduced by so-called swirl brakes. High pre-swirl speeds magnify the gas bearing effect when the whirling speed is lower than the rotating shaft speed, therefore the destabilizing effect is generally increased by pre-swirl speed.

In case of shrouded blade rows with labyrinth seals on top, the two destabilizing mechanisms of expressions (1) and (3) sum up, but due to interaction between them, the resultant destabilizing coefficient is not easy to be calculated and has been derived mainly from experimental results as shown by Pollman et al. [5]. They presented an overview of different excitation mechanisms, and compared calculated and measured excitation factors for 3 different types: single 50% reaction stage, 3 stage 50% reaction and impulse stage. The agreement is not very good, measured values are much higher than calculated values for the impulse stage, which is attributed to the gas bearing effect, are generally lower for the single 50% reaction stage and can be higher or lower for the 3 stage model, depending on pressure levels. Applications to real turbo-groups are also shown, and prediction of stable or unstable behaviour is claimed to be possible at design stage.

Benckert and Wachter [6] report accurate measurements made in different labyrinth seal geometries and attributes the destabilizing forces to swirl entry flow (for short seals) and to circumferential flow and related drag of rotating shaft (for long seals). These effects are shown separately. Linear behaviour is observed up to eccentricities of 40-60% of clearance, which is partially in contrast with the findings of Thomas et al. [3]. Results are applied successfully to steam turbines and compressors.

Calculations of stability margins in the design stage of steam turbines have been introduced in the design computer codes of steam turbine manufacturers [7]: these are based on the evaluation of the real part of the eigenfrequencies of the rotor system. For this calculation the evaluation of the excitation constant for each reaction blade row (with corrections for shrouded rows) and for the different types of labyrinth seals is based on the previously described research results. Seals and bearings, represented respectively by these cross coupling stiffnesses and by the stiffness and damping coefficients of the oil film bearings, constitute the connections between stationary casing and the rotating shaft, where they can cause unstable whirling motion, or stable behaviour.

Finally Hauck [8] and [9] resumes main excitations related to unequal circumferential pressure distribution in the seals of a deflected shaft, and to entry swirl. He presents accurate pressure and velocity measurements in the cavities between seal strips showing the presence of different flows: one mainly peripheral and another mainly axial. He shows also results of typical shrouded turbine stages with labyrinth seals.

Childs [10] describes exhaustingly all results obtained and models used in liquid and gas annular seals and turbine and pump impellers. Recently also CFD codes are available for analysing the behaviour of seals: test results are compared to calculated results obtained with two different CFD codes in Schettel and Nordmann [4], giving insight in capabilities of CFD codes to represent experimental results. They compare two CFD codes, one commercial and one developed in university, to experimental results. The two codes give quite different results, mainly because the labyrinth inlet and outlet geometries and conditions, to which the results are very sensitive, are taken into account in different ways. The results of both codes do not always fit the experimental results. The stiffness coefficients of (2) and (3) are strongly over or under estimated for different

pressure ratios at 0 pre-swirl, and for higher pre-swirl speeds. Anyhow predictions with CFD are claimed to be much more accurate with respect to bulk flow simulations.

A slightly different result has been found by Schettel et al. [11], where the experimental results of 17 different test conditions of a test rig designed expressly for these measurements, are compared to bulk flow method and CFD results. CFD calculation overestimates generally the stiffnesses of (2) and (3) by some amount, but bulk flow model gives wrong values of stiffness in (2) and acceptable values of stiffness in (3). Summarizing it seems that CFD calculations are more accurate but there are still some weak points in boundary conditions evaluation at inlet in seals, which can affect the accuracy of the calculation.

3. Steam whirl case history

The machine-train of a 425 MW power unit was composed of a single-flow high pressure turbine (HP), a single-flow intermediate pressure turbine (IP), a double-flow low pressure turbine (LP) and a generator. The shafts of the machine-train were directly coupled each other by means of rigid couplings. The operating speed of this reheat unit of reaction design was 3000 rpm. The steam admission to the HP section was full arc. The shaft-train was mounted on six main oil-film journal bearings having nearly the same geometrical properties. They were two-lobe journal bearings which showed two large pockets located at the horizontal partition of the bearing casing. The geometrical pre-load of the lower lobe was 0.3. Figure 3 shows the layout of the machine-train and the bearing numbers. Each support was equipped with a pair of XY proximity probes and one vertical seismic transducer.

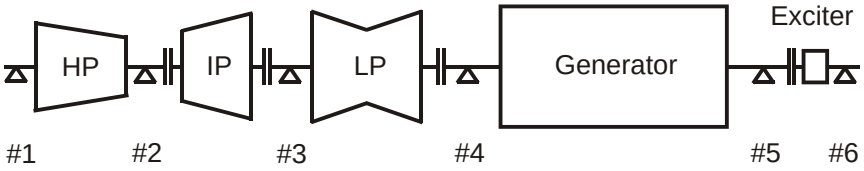

Figure 3: Machine-train layout and bearing numbers.

The HP turbine was mounted on two journal bearings whose lower lobe showed an angular width of only 60 degrees. The vibrations measured during a run down transient at bearing #1 (Figure 4) showed that the first critical speed of the HP turbine was split into two values: 1850 rpm and 1970 rpm.

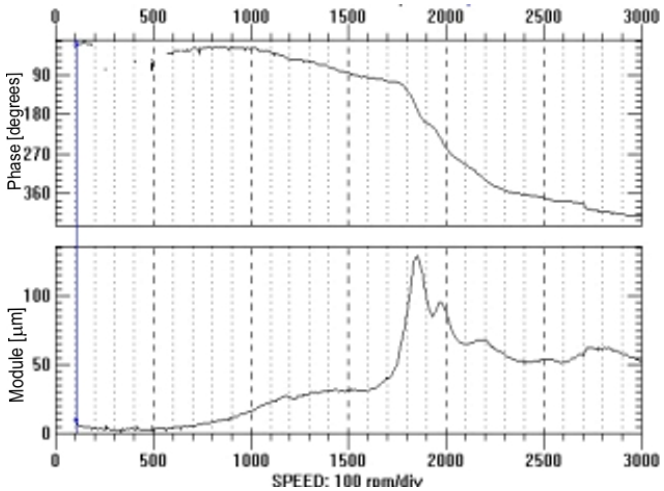

Figure 4: Synchronous transient vibrations (1X) measured at bearing #1 of the HP turbine: passing through the first critical speed.

Few months after the first rollout of the power unit the HP turbine showed multiple events of high vibration levels that occurred in operating condition and caused several machine trips. These high

vibrations always occurred when the electrical load exceeded the 80% of the nominal rating, that is when the opening degree of the main control valves of the HP section reached its upper range.

The vibrations measured at bearings from #3 to #6 were nearly unaffected by the abnormal vibrations that occurred at the bearings #1 and #2 of the HP turbine. The analysis of the harmonic content of the vibration signals showed that, in general, in occasion of each machine trip the amplitude of the synchronous component (1X) measured at 3000 rpm was not excessively high. On the contrary, few minutes before each machine trip a sub-harmonic component at 32 Hz suddenly appeared in the vibration signals. This value was rather close to the first flexural critical speed of the HP turbine. The amplitude of this component grew very quickly reaching considerable levels in less than 10 seconds.

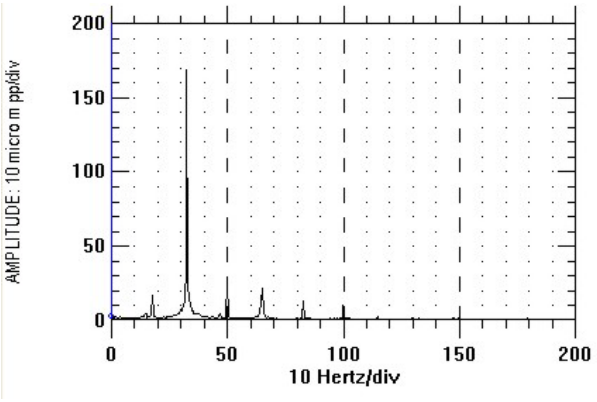

Figure 5: Spectrum of the shaft vibrations measured at bearing #1 in operating condition few seconds before the onset of the instability.

Figure 5 shows the frequency spectrum of the shaft vibrations measured at bearing #1 few seconds before the occurrence of a machine trip caused by the sharp growth of the amplitude of the sub-harmonic vibrations of the HP turbine. Figure 6 shows a waterfall diagram of the shaft vibrations measured at bearing #1 in occasion of one of the instability events. The orbit measured in the same bearing is shown in Figure 7: the subharmonic component tends to be quite circular, at least in the last two orbits, whilst the orbits in correspondence of on of the split critical speeds, shown in Figure 8, excited by the residual unbalance is more elliptical. Also this is a typical symptom of steam whirl: due to cross-coupled stiffness coefficients, two eigenvalues corresponding to the split critical speeds (shown in Figure 4) become equal and the orbit becomes circular. It is possible to note that the sub-harmonic vibrations immediately disappeared after the machine trip. The sudden and sharp increase of amplitude at constant speed when maximum power is approached, and still more the sudden and sharp disappearance of the subharmonic component when the power is removed are clear symptoms of steam whirl: other causes of instability (such as oil whirl) could be discarded. It was decided to check the stability margin calculation in design conditions.

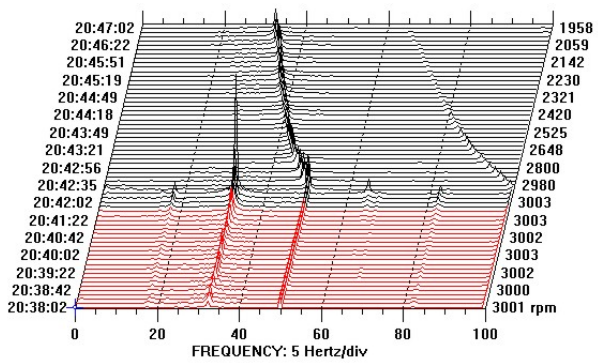

Figure 6: Waterfall plot of the shaft vibrations measured at bearing #1 in occasion of a steam-whirl instability onset and during the subsequent coast-down caused by the machine trip.

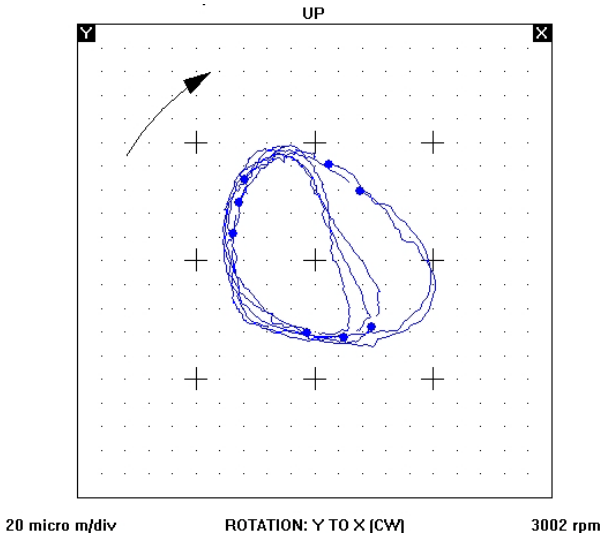

Figure 7: Orbit at onset of instability.

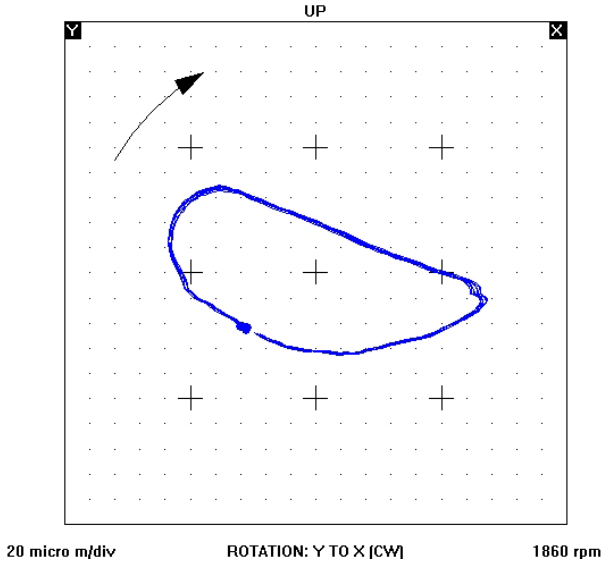

Figure 8: Orbits when passing critical speed.

4. Model of the machine and of the instability excitation

Figure 9 shows the finite element model of the rotor used to analyze its dynamic behaviour. The first phase of the analysis is checking the accuracy of the model of the machine. The unbalance response in bearing 1 of the machine has been calculated without considering the effect of the seals, simulating the start up of the machine without electrical load.

Equation (4) is the standard frequency response matrix equation that is obtained as described in [16]:

$$[\mathbf{M}]\ddot{\mathbf{x}} + \left([\mathbf{R}] + [\mathbf{G}(\Omega)]\right)\dot{\mathbf{x}} + [\mathbf{K}]\mathbf{x} = \mathbf{F}(t) \tag{4}$$

where $[\mathbf{M}]$ is the mass matrix, $[\mathbf{R}]$ the damping matrix, $[\mathbf{G}]$ the gyroscopic matrix, $[\mathbf{K}]$ the stiffness matrix. The system is here solved using the rotor dynamics software RAFT, developed by Department of Mechanics – Politecnico di Milano.

The stiffness matrix $[\mathbf{K}]$ is assembled using the superposition of the stiffness matrices of the shaft train, journal bearings and supporting structure.

$$[\mathbf{K}] = [\mathbf{K}]_{shaft-train} + [\mathbf{K}]_{bearings} + [\mathbf{K}]_{foundation} \tag{5}$$

The shaft train stiffness matrix $[\mathbf{K}]_{shaft-train}$ is obtained by means of the typical methods for rotor modelled by finite beam elements (see [15][16]), which allow the matrix coefficients to be defined. Bearing and supporting structure matrices $[\mathbf{K}]_{bearings}$ and $[\mathbf{K}]_{foundation}$ are assembled as described in [16]. The coefficients in these matrices are given by the machine manufacturer.

Similarly, the damping matrix $[\mathbf{R}]$ includes the contribution of the structural damping of the shaft train, that of the journal bearings and that of the supporting structure.

$$[\mathbf{R}] = [\mathbf{R}]_{shaft-train} + [\mathbf{R}]_{bearings} + [\mathbf{R}]_{foundation} \tag{6}$$

Again, the coefficients in matrices $[\mathbf{R}]_{bearings}$ and $[\mathbf{R}]_{foundation}$ are supplied by the manufacturer.

If bearing stiffness and damping parameters were not available, but journal bearing geometry, loads and operating conditions were known, they could be calculated using methods exposed e.g. in [17].

Unbalance of 1 kgm has been applied in the middle of the HP shaft, in order to excite its first critical speed. Figure 10 shows the results: the agreement with experimental results of Figure 4 in critical speed value, and in the associated damping proves that the model is satisfactory.

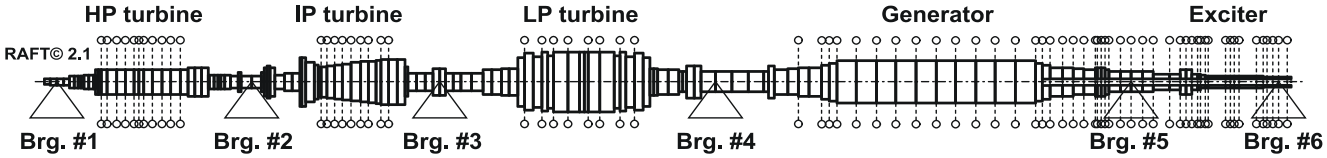

Figure 9: Finite element model of the turbo-generator.

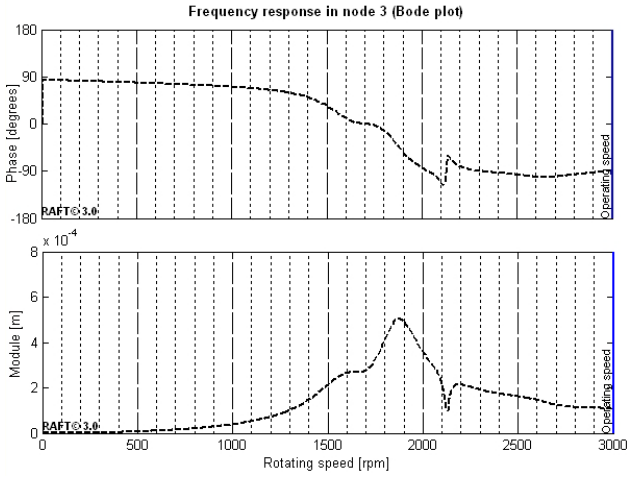

Figure 10: Unbalance response in bearing 1 of HP steam turbine.

The second phase of the analysis schedules the stability checking, considering the effects of the seals. According to the procedure described in [7], only the cross coupling stiffnesses of (1) and (3) have been considered, other effect of the seals on the system stiffness and damping have been neglected. This implies that a further term is added to the system stiffness matrix:

$$[\mathbf{K}] = [\mathbf{K}]_{shaft-train} + [\mathbf{K}]_{bearings} + [\mathbf{K}]_{seals} + [\mathbf{K}]_{foundation} \tag{7}$$

where the stiffness matrix $[\mathbf{K}]_{seals}$ of the seals is assembled considering the stiffness matrices associated to each seal, as shown hereafter.

The swirl speed has been assumed half of the value of the shaft surface speed. For the shrouded blade rows the combined effect of (1) and (3) is roughly extrapolated from results of few experimental values. With these assumptions, the values of the cross coupled stiffnesses, in

correspondence of all blade rows and all labyrinth seals of the HP turbine only shown in Figure 11, have been obtained.

The cross-coupled coefficients are supplied by the manufacturer that calculated them according to the procedure described in [7] based on the approach described in [4] for the blades, on bulk flow theory for the labirynth seals and on some experimental results for the shrouded blades with labyrinths on top. Each pair of cross-coupled coefficients, having the same magnitude and opposite sign, is assembled in the off-diagonal locations of the stiffness matrix associated with the *j*-th seal. In a fixed frame coordinate system *xy* this matrix can be written as:

$$\left[\mathbf{K}_s\right]_j = \begin{bmatrix} 0 & k_{xy} \\ k_{yx} & 0 \end{bmatrix}_j, \; k_{yx} = -k_{xy} \tag{8}$$

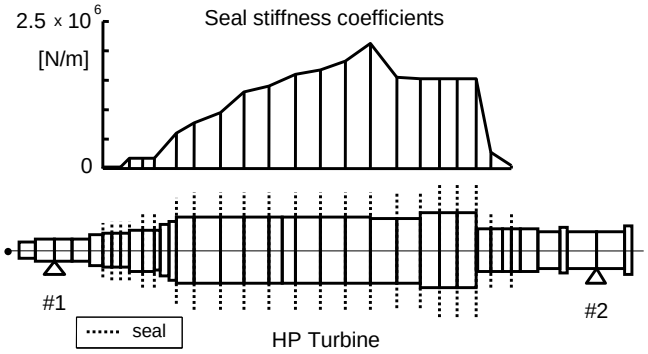

Figure 11: Nominal absolute values of the seal stiffness coefficients provided by the machine manufacturer.

As shown in expression (1) the stiffness over the blade rows is proportional to the power, giving rise to the highest excitation in maximum power conditions. Therefore, at high power levels the cross-coupled stiffness terms of the matrices defined by eq. (1) can be responsible for self-excited rotor instability phenomena characterized by a subsynchronous shaft whirl that is associated with the first flexural normal mode of the rotor. The analysis of the eigenvalues of the rotating machine model can be used to point out the conditions that must be satisfied for the occurrence of unstable vibrations.

The *k*-th eigenvalue of the model can be written as:

$$\lambda_k = \sigma_k + \mathrm{i}\, 2\pi f_{dk} \tag{9}$$

where f_{dk} is the *k*-th damped natural frequency of the system while σ_k is the respective modal damping factor. In order to have energy dissipation the factor σ_k must be negative. The respective undamped natural frequency is given by:

$$f_{nk} = \frac{1}{2\pi}\sqrt{\left(2\pi f_{dk}\right)^2 + \sigma_k^2} \tag{10}$$

The *k*-th dimensionless damping factor, h_k, can be expressed in the following form:

$$h_k = -\sigma_k \big/ \left(2\pi f_{nk}\right) \tag{11}$$

In order to have oscillating motions the dimensionless damping factor must be positive and lower than the unity. Under the assumption that the rotor system vibrates in the free motion with an harmonic law having a frequency equal to the *k*-th damped natural frequency f_{dk}, the time history of the displacements evaluated at the *j*-th degree of freedom x_j can be written as:

$$x_j(t) = X_j\, \mathrm{e}^{-h_k 2\pi f_{nk} t} \cos(2\pi f_{dk} t + \varphi_j) \tag{12}$$

Let us denote T_k the time period associated with the damped natural frequency f_{dk}. The instability factor V_k can be expressed by the ratio between the vibration amplitudes evaluated at the two instants t_1 and t_2 which satisfy the following relationship: $t_2 = t_1 + T_k$:

$$V_k = \frac{x(t_2)}{x(t_1)} \tag{13}$$

If the free motion is actually damped then $x(t_2) < x(t_1)$ and $V_k < 1$. The instability factor, considering also eqs. (10) and (11), results:

$$V_k = \frac{e^{-h_k 2\pi f_{nk}(t_1+T_k)}}{e^{-h_k 2\pi f_{nk} t_1}} = e^{-h_k 2\pi f_{nk} T_k} = e^{-h_k 2\pi \frac{f_{nk}}{f_{dk}}} = e^{-\frac{2\pi h_k}{\sqrt{1-h_k^2}}} \tag{14}$$

In alternative form, the logarithm of the instability factor is given by:

$$\ln(V_k) = -2\pi h_k \Big/ \sqrt{1-h_k^2}\ ,\ V_k < 1 \tag{15}$$

When the instability factor V_k exceeds the unity, the rotating machine can be affected by instability phenomena.

The sensitivity of the machine-train to the values of the seal stiffness coefficients regarding the occurrence of steam-whirl instability phenomena caused by the seal excitation constant has been investigated. This study has been carried out by multiplying all the nominal values of the seal stiffness coefficients of the model by a scaling factor, c_s. Different analyses have been performed by varying this scaling factor from 0 to 3. The null value of c_s can be associated with the off-load condition while the unity value of c_s corresponds to the full-load operating condition. For each value assigned to the constant c_s the eigenvalues of the machine model have been evaluated. The real part of each eigenvalue has been used to calculate the instability factor V associated with each flexural critical speed of the shaft-train. Instability factors that exceed the unity indicate the presence of conditions that can cause the occurrence of steam-whirl instability phenomena. Table 1 shows the flexural critical speeds in which the HP steam turbine is involved and the respective instability factors of the machine-train evaluated at the operating speed without considering the stiffness of the seals. The damping of the oil film bearings lowers the instability factor of mode 6 of the complete group (which is also the first mode of the HP steam turbine rotor) to 0.79, which is sufficiently below the unity threshold.

TABLE 1: Flexural critical speeds and instability factors evaluated at 3000 rpm, without considering the stiffness of the seals (off-load operating conditions: c_s = 0).

Mode n.	Flexural Critical Speed [rpm]	Instability Factor (V)	Mode n.	Flexural Critical Speed [rpm]	Instability Factor (V)
5	1781	0.8862	6	1853	0.7964

If the effect of the seals is considered, in design conditions (c_s=1.0) the instability factor is still 0.81, as shown in Figure 12. Instability should not occur. Only when the scaling factor reaches 2.15 the damping factor approaches unity, and the rotor becomes unstable. This indicates a good stability margin. The only mode which becomes unstable is the 6th mode of the group, which is also the first mode of the HP turbine shaft.

The results provided by this case study, using the machine nominal model, do not explain the reason for the occurrence of steam-whirl instability phenomena.

In order to check the accuracy of the eigenvalue calculation, also another approach has been used, based on energy balance [12]. A whirling motion at critical speed is imposed by a rotating force; the energies introduced by seals and dissipated by damping in bearings can be evaluated considering

the different elliptical orbits in the different locations. If the net energy is positive the system is unstable, if negative stable.

This method could be more robust with respect to eigenvalue calculation. It would also allow to localize the seals which contribute more to the onset of instability, or the bearings which contribute more to stability. This calculation showed exactly the same results: a good stability margin in design conditions. Therefore the loss of stability and the discrepancy between experimental findings and model results was attributed to errors in bearing and seal coefficients evaluation, and an analysis was made for trying to detect where modelling errors have occurred.

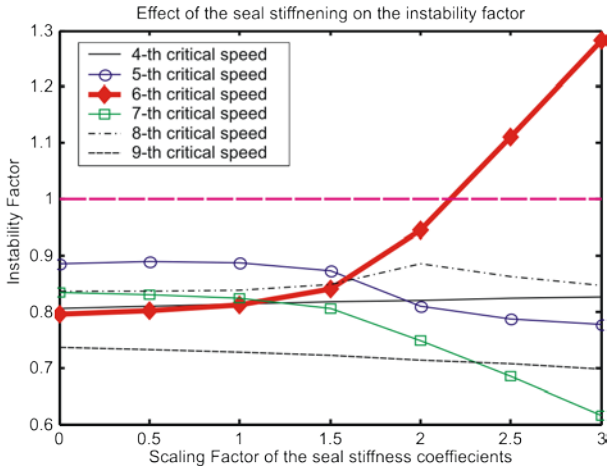

Figure 12: Instability factor versus exciting constant scaling factor.

5. Accuracy of actual stability calculations of steam turbines

The results of this calculation shows that calculations made using well assessed procedures for standard design machines are insufficient to avoid steam whirl conditions: this could be attributed to some modelling inaccuracies which have not been recognized.

Analysing the standard approach for calculating stability margins of steam turbines one could find following aspects which are neglected, or taken into account by more or less rough approximations or interpolations.

Oil film bearings: the damping coefficients of oil film bearings can be affected significantly by bearing misalignment, by higher oil film temperature with respect to design, and by deviations from design geometry.

Labyrinth seals and shrouded blade row seals: the excitation coefficient for these seals is calculated assuming standard fluid dynamic behaviour. This means that:

a. The circumferential fluid velocity distribution across the clearance is considered linear (as shown in Figure 2). The effect of higher velocities due to swirl components in circumferential direction are therefore neglected.
b. flow contraction and carry over flow are also neglected.
c. differences due to the dynamic behaviour of the fluid around a whirling shaft instead of eccentric rotating shaft are neglected, because the experiments had mainly been made with eccentric rotating shafts (as reported in [8][9][13]) rather then with whirling shafts (see [14]).
d. The “gas bearing” effect due to shrouds on the blade row is represented by a corrective factor which is interpolated between some few experimental results.
e. Non linearity are not taken into account, therefore:
f. The effect of misalignment of shaft with respect to casing, as well as the resulting unequal pressure and velocity distributions in the seal is not considered.
g. The effect of actual orbit size and shape in correspondence of each seal is also completely neglected.

h. Effect of different operating conditions with respect to design have not been considered.

It seems reasonable to decouple the onset of instability from steady state vibrational behaviour, but considering the non-linearity in seals and bearings it could also result that a strong 1X component in bearings and seals, due to unbalance and bow, would be able to overcome the onset of instability.

6. Conclusions

A case history about steam whirl instability in a steam turbo generator is presented and discussed, modelling the phenomenon. In the same plant, another machine of the same design did not show any instability. Therefore the onset of the instability must depend on the destabilizing effects of some parameters which are not completely controlled during the installation of the machine. Actual clearances could be different in the two machines due to tolerances. The alignment of the bearings in hot condition, which define also the position of the shaft with respect to the stator, could also be different in the two machines. Loads on the bearings may change with the alignment and therefore also the damping coefficients of the oil film, as well as the velocity and the pressure distributions may change in the seal due to the eccentricity of the rotor. The actual velocity and pressure distribution in correspondence of the labyrinth seals, which could be different from design, influences the pre-swirl velocity, which affects strongly the destabilizing forces.

Only CFD calculations and accurate measurements of actual values of the geometrical parameters, such as clearances and alignment conditions, could improve the accuracy of steam whirl stability calculations.

References

[1] Thomas, H.J., Instabile Eigenschwingungen von Turbinenlaeufern, angefacht durch die Spaltstroemungen in Stopfbuchsen und Beschaufelungen (Unstable vibrations of turbine rotors excited by clearance flows in sealings and bladings), Bull. De l'AIM, 71, n.11/12, 1039-1064 (1958).

[2] Krämer, E., Selbsterregte Schwingungen von Wellen infolge Querkraefte (Self-excited vibrations of shafts due to transverse forces), Brennst.-Waerme-Kraft, 20, n.7 (1968).

[3] Thomas, H.J., Urlichs, K., Wohlrab, R., Laeuferinstabilitaet bei thermischen Turbomaschinen infolge Spalterregung (Rotor instability in thermal turbomachinery due to clearance excitation), VGB Kraftwerkstechnik, 56, n.6 June 1976, 377-383 (1976).

[4] Schettel, J., Nordmann, R., Rotordynamics of turbine labyrinth seals - a comparison of CFD models to experiments, IMechE paper C623/018, 13-22 (2004).

[5] Pollman, E., Schwerdtfeger, H., Termuehlen, H., Flow excited vibrations in high pressure turbines (Steam whirl), ASME J. of Eng. for Power, 100, 219-228 (1978).

[6] Benckert, H., Wachter, J., Flow induced spring constants of labyrinth seals, IMechE paper C258/80, 53-63 (1980).

[7] Stability calculation overview, ABB (1994).

[8] Hauck, L., Measurement and evaluation of swirl-type flow in labyrinth seals of conventional turbine stages NASA Conference Publication, 242-259 (1982).

[9] Hauck, L., Vergleich gebraeuchlicher Tubinenstufen hinsichtlich des Auftretens spaltstroemungsbedingter Kraefte (Comparison of usual turbine stages as regards clearance flow induced forces), Konstruktion 33, n.2, 59-64 (1981).

[10] Childs, D., Turbomachinery Rotordynamics: phenomena, modeling and analysis, John Wiley & Sons, (1993).

[11] Schettel, J., Lueneburg B., Deckner M., Mynott H., Validating a steam whirl design procedure for steam turbine –generator sets for power generation, 7th IFToMM Conference on Rotordynamics, Vienna, Austria, 25-28 Sept. (2006).

[12] Diana, G., Massa, E., Pizzigoni, B., Marcantoni-Taddei, C., A forced vibration method to calculate the oil film instability threshold of rotor-foundation systems, IFToMM Interantional Conference on Rotordynamic Problems in Power Plants, Rome, Italy, 28 Sept. – 1 Oct. (1982).

[13] Benckert, H., Wachter, J., Flow induced spring constants of labyrinth seals, IMechE paper C258/80, 53-63 (1980).

[14] Kwanka, K., Ortinger, W., Rotordynamic coefficients of long staggered labyrinth gas seals, International Journal of Rotating Machinery, 1, n.3-4, 285-291 (1995).

[15] Lalanne, M. and Ferraris, G., Rotordynamics Prediction in Engineering. John Wiley & Sons Inc, Chichester, England (1988).

[16] Pennacchi, P., Bachschmid, N., Vania, A., Zanetta, G.A. and Gregori, L., Use of modal representation for the supporting structure in model based fault identification of large rotating machinery: part 1 – theoretical remarks. Mechanical Systems and Signal Processing, 20(3), pp. 662-681 (2006).

[17] Someya T., Journal-Bearing Databook, Springer-Verlag (1989).